Nanoindentation-induced amorphization in silicon carbide

Izabela Szlufarska,[a] Rajiv K. Kalia, Aiichiro Nakano, and Priya Vashishta
*Collaboratory for Advanced Computing and Simulations, Department of Materials Science,
Department of Physics, Department of Computer Science, University of Southern California, Los Angeles,
California 90089-0242*

The nanoindentation-induced amorphization in SiC is studied using molecular dynamics simulations. The load-displacement response shows an elastic shoulder followed by a plastic regime consisting of a series of load drops. Analyses of bond angles, local pressure, and shear stress, and shortest-path rings show that these drops are related to dislocation activities under the indenter. We show that amorphization is driven by coalescence of dislocation loops and that there is a strong correlation between load-displacement response and ring distribution. © *2004 American Institute of Physics.* [DOI: 10.1063/1.1774252]

Silicon carbide (SiC) is a material of great scientific and technological interest[1] for the fabrication of electronic and optoelectronic devices. Among many crystal structures of SiC the most common is the cubic (zinc-blende) polytype denoted as $3C-SiC$.

Nanoindentation is a powerful and widely used technique to access the mechanical properties of materials.[2–6] There has been a large number of experimental[7] and computational[8] studies of the indentation-induced crystalline to amorphous $(c \rightarrow a)$ transformation. It has been suggested that the nanoindentation load-displacement $(P-h)$ response is correlated with the subsurface defect nucleation,[9–12] and experimental evidence was provided[13] that dislocation activity leads to amorphization during indentation of silicon. However, the microscopic mechanism of amorphization is not known. The $c \rightarrow a$ transformation is initiated on the atomic scale and the need for its atomic-level description is critical. Atomistic simulations based on molecular dynamics[14] (MD) provide trajectories of all the atoms and have been already employed in nanoindentation studies[12,15–17] to bring atomistic insight into the mechanisms of defect nucleation at the initial stages of plastic activity. Therefore MD simulations are expected to shed light on the atomistic pathway to amorphization via nanoindentation.

In this letter we study by means of MD the atomic-scale mechanisms governing the indentation-induced amorphization of $3C-SiC$. At a small displacement a reversible pop-in behavior in the $P-h$ curve is observed, indicating a remarkable elastic recovery of $3C-SiC$. This is followed by the plastic regime, in which we observe a series of load drops, which are related to subsurface dislocation activities. We characterize these structural deformations in terms of bond angles, local shear stress and pressure, spatial distribution of atoms, and shortest-path-ring distribution. We demonstrate how the ring analysis can be effectively employed to study nanoindentation damage. Simulation results reveal that the defect stimulated growth and coalescence of dislocation loops play an important role in indentation-induced amorphization.

The potential used in our study is a combination of two- and three-body interaction terms, which include steric repulsion, van der Waals interaction, electronic polarizability, charge transfer, and covalent bondings effects. Calculated lattice constant, melting temperature, and elastic constants are in good agreement with experiments. This potential was used earlier to predict a new mechanism for a reversible zinc-blende to rocksalt transformation of SiC under pressure.[18]

The simulated system consists of 994 000 atoms in a $308.3 \times 309.5 \times 107.9$ Å^3 crystal in the x, y, and z directions, corresponding to the $[\bar{1}10]$, $[001]$, and $[110]$ crystallographic directions, respectively. Periodic boundary conditions are applied in the x and y directions, whereas z is the indent direction. The SiC indenter is rigid and it has a flat square base of dimensions 30.8×30.5 Å^2 and a height of ~ 60 Å. The interaction between the atoms of the indenter and the substrate is purely repulsive. The indenter is inserted up to $\sim 10\%$ of the substrate thickness at a rate of 100 m/s. Each 0.5 Å depth increment is followed by a holding phase of ~ 17.6 ps to allow the decay of transient forces.

The calculated load-displacement $(P-h)$ curve is shown in Fig. 1(a). A characteristic feature of this curve is a series of sudden load drops, of which the first one occurs at $h = 2.83$ Å and all the other are equally spaced by ~ 3 Å. The drops of the load correspond to breaking of subsequent atomic layers of the underlying substrate, which in the z direction are separated by 3.08 Å. The $P-h$ curve also exhibits a shoulder at $h = 0.83$ Å. An insight into the nature of this shoulder as well as of the first load drop is brought by performing two unloading simulations [see Fig. 1(b)], in which we gradually remove the indenter from the depths (1)
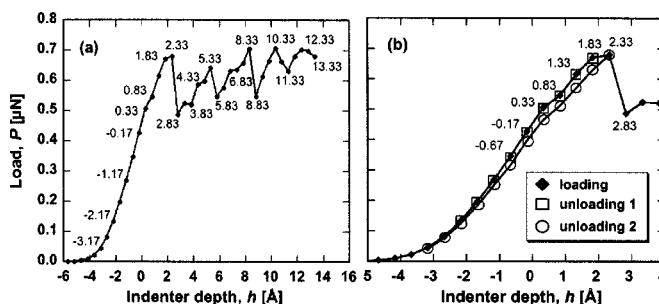

FIG. 1. (a) Load-displacement $(P-h)$ curve. (b) Unloading curves from depths (1) $h = 1.83$ Å (squares) and (2) $h = 2.33$ Å (circles).

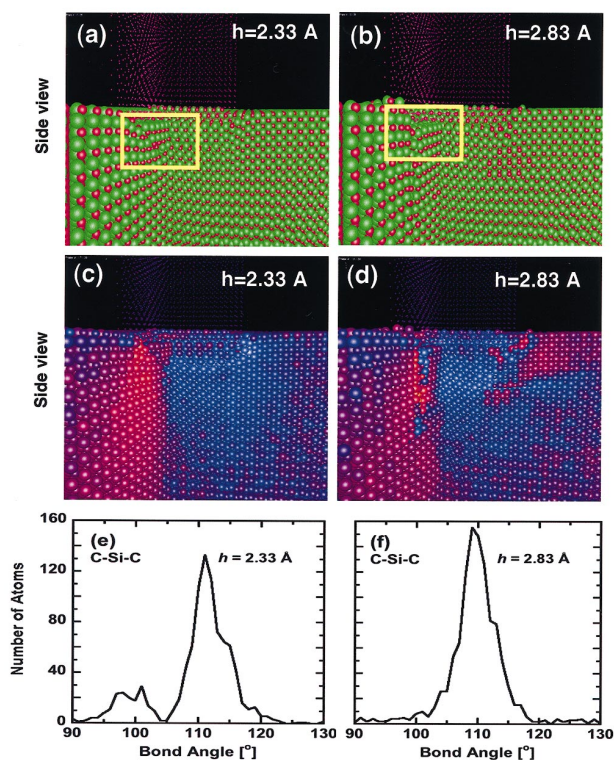[a]Electronic mail: izabela@usc.edu

FIG. 2. (Color) (a), (b) 3/4 cut showing atomic species under the indenter at $h=2.33$ Å and $h=2.83$ Å (c), (d) 3/4 cut view of shear stress at $h=2.33$ Å and $h=2.83$ Å (e), (f) Bond angle distribution at indenter depths $h=2.33$ Å and $h=2.83$ Å.

FIG. 3. (Color) Ring distribution analysis: atoms with non-threefold rings at $h=11.33$ Å.

$h=1.8$ Å (squares) and (2) $h=2.33$ Å (circles). Because the first unloading curve retraces exactly the loading path (closed diamonds), we confirm the elastic character of the shoulder at $h=0.83$ Å. The second unloading curve does not follow the loading path, which indicates the onset of plastic deformation at $h=2.33$ Å. Correspondingly, the yield strength of the crystal equals ~77 GPa.

We analyze the relation between the $P-h$ response and the structural changes in the substrate at every point along the $P-h$ curve. Figures 2(a) and 2(b) show the side view of the atomic species under the indenter at $h=2.33$ Å and $h=2.83$ Å, respectively. As shown in the region marked by a yellow rectangle, pushing the indenter into the solid down to the depth of $h=2.33$ Å results in bending of atomic layers. This process continues until finally the load becomes critical causing the atomic layers to slip at $h=2.83$ Å [Fig. 2(b)]. The slip of atomic planes is repeated at $h=5.83, 8.83,$ and 11.33 Å, that is every time the load in Fig. 1 significantly drops.

We also characterize the $P-h$ response by distribution of the local shear stress. As shown in Fig. 2(c) for $h=2.33$ Å, before the slip there is a high concentration of shear stress in the region of interest, whereas after the slip [Fig. 2(d)] a considerable amount of the shear stress is released. Similar behavior is observed at higher indentation depths, however due to the presence of more complex deformation structures (merging of dislocation loops) the relaxation of shear stress is not as dramatic. This also explains why in Fig. 1 the drops of the load at large h are smaller than at $h=2.33$ Å

Structural defects are further analyzed by calculating C–Si–C and Si–C–Si bond angle distribution in the selected region under the indenter (12–17 Å below the initial
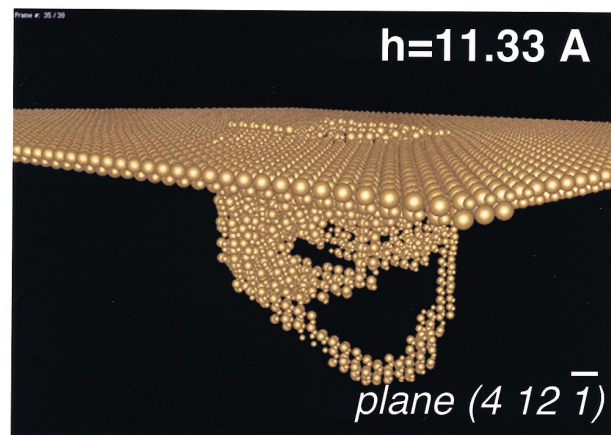
surface). In the zinc-blende crystal both of these distributions exhibit a sharp peak at ~109° due to the perfect tetrahedral arrangements of atoms. The distributions are significantly broadened in the amorphous phase, *a*-SiC. In our simulation, bringing the indenter closer to the substrate results in distortion of the tetrahedral arrangements of atoms and in splitting of the single peak in bond angle distribution [see Fig. 2(e)]. Remarkably, after the slip of atomic layers has taken place, the single peak structure in the bond angle distribution is restored [Fig. 2(f)]. Even though a similar behavior is observed at higher indentation depths, in those cases the distribution is noticeably broadened. This is once again due to a more complex subsurface deformation structure and thus only partial relaxation of accumulated shear stress.

The correlation between the drops in the $P-h$ response and the subsurface deformations is further investigated by means of the shortest-path ring distribution. In a zinc-blende crystal the occurrence of structural deformations is marked by the presence of non-threefold rings.[19] We find that down to the depth of $h=0.33$ Å there are only threefold rings in the substrate. The small amount of non-threefold rings that appears at the shoulder at $h=0.83$ Å disappears upon unloading, which confirms the elastic character of the shoulder. Irreversible non-threefold rings occur at $h=2.33$ Å, that is at the onset of plastic deformation. At $h=2.83$ Å, where both the atomic layers slip [Fig. 2(b)] and the load drop (Fig. 1) take place, we observe an outburst of dislocations and dislocation loops emitted from the corners of the indenter and disconnected from one another. During the further lowering of the indenter the dislocation loops slowly grow on the {111} planes, which are the glide planes in the zinc-blende crystal. In fact, every time the load drops in the $P-h$ response, such outburst of non-threefold rings takes place. For $h=5.83$ Å and larger, these dislocation loops start to coalesce. At $h=8.83$ Å there is a dislocation loop that appears on the $(2\,2\,\bar{1})$ plane. Lowering the indenter further causes this loop to grow until at $h=11.33$ Å it coalesces with newly emitted deformations and forms a new loop on the $(4\,12\,\bar{1})$ plane (see Fig. 3).

Our analysis suggests that the coalescence of the dislocation loops is responsible for the broadening of bond angle and a decrease of the magnitude of shear stress released at $h=5.83$ Å as compared to $h=2.83$ Å. In Fig. 4(a) the bond angle distribution at $h=11.33$ Å is compared with that of a
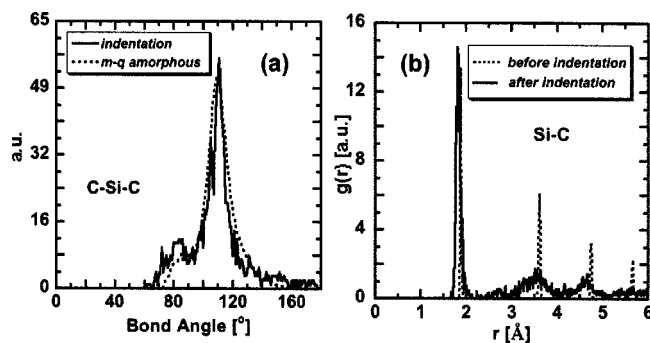
FIG. 4. (a) Bond angle distribution: solid line—substrate material under the indenter at $h=11.33$ Å: dashed line—melt-quenched (m–q) bulk amorphous. (b) Radial distribution function before and after indentation.

melt-quenched amorphous system. The two curves are very similar, showing a wide bond angle distribution from 70° to 160°. This is a clear indication that the material beneath the indenter became amorphous. In Fig. 4(b) we plot the radial distribution function before and after indentation to show the transition from crystalline to amorphous structure.

Evidently, there is a correlation between the load drops in the $P-h$ response and the emission of dislocations identified by means of ring distribution. In order to quantify this correlation, in Fig. 5 we plot together the load on the indenter and the number, δN, of atoms with non-threefold rings as a function of h. In the calculation of δN we omit a linear term that is due to the atoms directly surrounding the in-
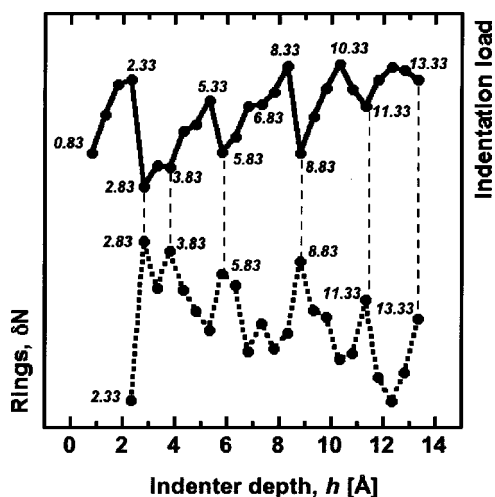

FIG. 5. The load-displacement response $P-h$ (solid line) and number $\delta N(h)$ of atoms with non-threefold rings (dotted line).

denter. Clearly, every time when the load drops, there is an increase in the number of non-threefold rings (the vertical dashed lines are added for emphasis). Ring analysis thus proves to be a powerful technique to study the nanoindentation damage.

In summary, we performed MD simulations to study the atomic-level mechanisms controlling the nanoindentation-induced amorphization in SiC. In the elastic regime the calculated $P-h$ curve exhibits a shoulder, which is fully reversible upon unloading. In the plastic regime the $P-h$ curve is characterized by a series of load drops and their relation to the subsurface crystalline structure and dislocation dynamics has been shown. This relation has been analyzed by means of bond angles, local shear stress, local pressure, and spatial rearrangements of atoms. We have demonstrated how the shortest-path-ring analysis can be effectively employed to study the evolution of indentation damage and defect accumulation beneath the indenter. These structural analyses reveal that the defect stimulated growth and dynamics of dislocation loops are responsible for the $c \rightarrow a$ transition.

[1] D. C. Pender and N. Padture, J. Mater. Sci. Lett. **17**, 999 (1998).
[2] J. Knap and M. Ortiz, Phys. Rev. Lett. **90**, 226102 (2003).
[3] G. S. Smith, E. B. Tadmor, and E. Kaxiras, Phys. Rev. Lett. **84**, 1260 (2000).
[4] G. M. Pharr, W. C. Oliver, and D. S. Harding, J. Mater. Res. **6**, 1129 (1991).
[5] M. F. Doerner and W. D. Nix, J. Mater. Res. **1**, 601 (1986).
[6] J. J. Kruzic and R. O. Ritchie, J. Am. Ceram. Soc. **86**, 1433 (2003).
[7] D. R. Clarke, M. C. Kroll, P. D. Kirchner, and R. F. Coof, Phys. Rev. Lett. **60**, 2156 (1988).
[8] J. S. Kallman, W. G. Hoover, C. G. Hoover, A. J. De Groot, S. M. Lee, and F. Wooten, Phys. Rev. B **47**, 7705 (1993).
[9] A. Gouldstone, K. J. V. Vliet, and S. Suresh, Nature (London) **411**, 656 (2001).
[10] C. L. Kelchner, S. J. Plimpton, and J. C. Hamilton, Phys. Rev. B **58**, 11085 (1998).
[11] J. Li, K. J. V. Vliet, T. Zhu, S. Yip, and S. Suresh, Nature (London) **418**, 307 (2002).
[12] J. A. Zimmerman, C. L. Kelchner, P. A. Klein, J. C. Hamilton, and S. M. Foiles, Phys. Rev. Lett. **87**, 165507 (2001).
[13] M. Tachi, Suprijadi, S. Arai, and H. Saka, Philos. Mag. Lett. **82**, 133 (2002).
[14] T. Cagin and J. R. Ray, Phys. Rev. A **37**, 247 (1988).
[15] U. Landman, W. D. Luedtke, N. A. Burnham, and R. J. Colton, Science **248**, 454 (1990).
[16] D. W. Brenner, S. B. Sinnott, J. A. Harrison, and O. A. Shenderova, Nanotechnology **7**, 161 (1996).
[17] E. B. Tadmor, R. Miller, and R. Phillips, J. Mater. Res. **14**, 2233 (1999).
[18] F. Shimojo, I. Ebbsjo, R. K. Kalia, A. Nakano, and P. Vashishta, Phys. Rev. Lett. **84**, 3338 (2000).
[19] J. P. Rino, I. Ebbsjö, P. Branicio, R. K. Kalia, A. Nakano. and P. Vashishta (unpublished).